Component separation with COrE-PRISM: some ideas

Mathieu Remazeilles

The University of Manchester

COrE/PRISM workshop, 10-11 Feb 2014, Paris

Advantages of COrE/PRISM satellite

Much larger number of frequency channels

good for separating much more components

high sensitivity

good for extracting faint signals:

- primordial CMB B-modes
- kinetic SZ
- relativistic thermal SZ

However

Component separation results become much more sensitive to incorrect prior assumptions on foreground models

Lack of information on polarized foregrounds

- Spectral indices of the polarized foregrounds?
  - may vary over sky
  - may vary over scale
- How many polarized foreground components in the sky?
  - thermal dust
  - synchrotron
  - spinning dust ?
  - ... ?

Answer not only depends on physics but also on the local noise level

These unknowns define our priors for component separation!

Errors on foreground modelling propagate to (τ, r) estimation

Collection of different component separation methods

We already have strong expertise and success from Planck:

Method	type	domain	targets
Commander	Bayesian parametric	pixel space	CMB, foregrounds
NILC	non-parametric	wavelet space	CMB, SZ
SMICA	“blind” (ICA)	harmonic space	CMB, SZ

All methods rely on prior assumptions on foregrounds

ex: “blind” SMICA makes prior assumption on the number of foregrounds

Targeting the signal subspace

Remazeilles, Delabrouille, Cardoso (2011)

Model of T,E,B data covariance matrix:

$$\mathbf{R} = \mathbf{R}_{FG} + \mathbf{R}_{CMB} + \mathbf{R}_{noise}$$

- $\mathbf{R}_{noise}$ can be computed from jackknife

$$\mathbf{R}_{noise}^{-1/2}\,\mathbf{R}\,\mathbf{R}_{noise}^{-1/2} = \mathbf{R}_s + \mathbf{I}$$

- $\mathbf{R}_s$: sky signal (CMB + foregrounds)
- $\mathbf{I}$: whitened noise (identity matrix)

Eigenstructure of $\mathbf{R}_{noise}^{-1/2}\,\mathbf{R}\,\mathbf{R}_{noise}^{-1/2}$:

$$\left[\begin{array}{c|c} \mathbf{U_S} & \cdots \end{array}\right] \cdot \left[\begin{array}{ccc|c} \lambda_1 + 1 & & & \\ & \cdots & & \\ & & \lambda_m + 1 & \\ \hline & & & \mathbf{I} \end{array}\right] \cdot \left[\begin{array}{c} \mathbf{U_S}^T \\ \hline \cdots \end{array}\right]$$

n frequency channels versus *m* sky degrees of freedom (rank-$(m\text{-}1)$ FG covariance matrix)

Maximum likelihood solution minimizing the spectral mismatch, a la SMICA

Generalised NILC (G-NILC) *Remazeilles, Delabrouille, Cardoso, MNRAS (2011)*

Going beyond SMICA by model selection:
What is the effective number m of polarized foregrounds?

Minimizing the Akaike Information Criterion (AIC) makes the trade-off "goodness of fit of the model" vs "complexity of the model"

$$AIC(m) = p(m) - 2 \log \mathcal{L}_{max}(m) \quad (1)$$

→ the AIC penalty $p(m) = 2m$ selects the best value of the rank m^*

→ Estimated locally in space and in scale using wavelets

Maps of the number of foregrounds (Planck-like)

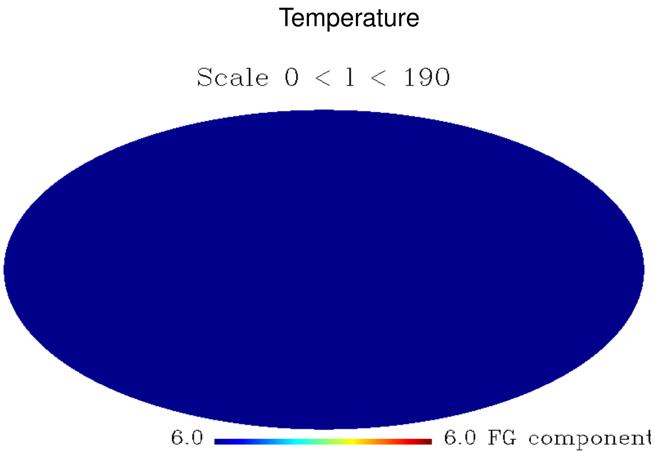

G-NILC able to provide maps of the number of foregrounds over the sky

Maps of the number of foregrounds (Planck-like)

temperature

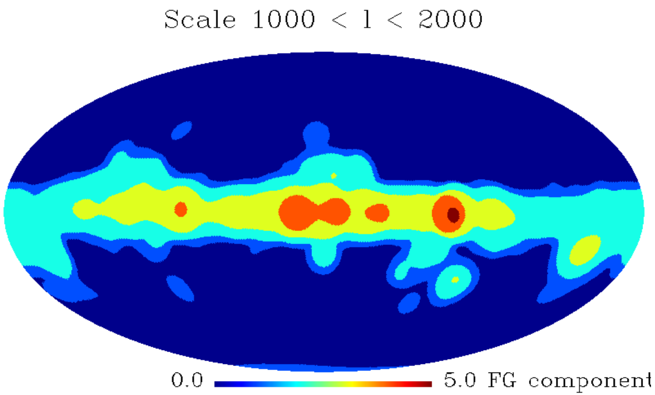

G-NILC able to provide maps of the number of foregrounds over the sky

Maps of the number of foregrounds (Planck-like)

Temperature

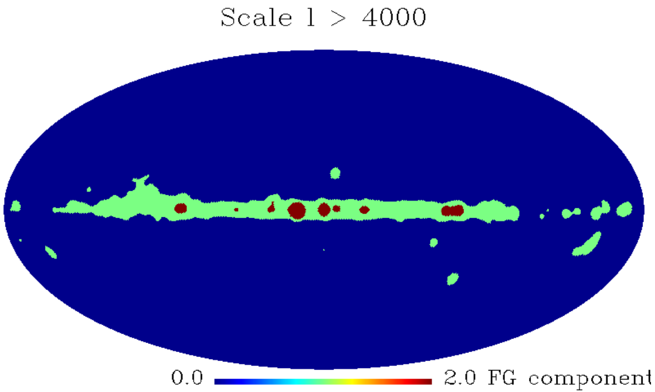

G-NILC able to provide maps of the number of foregrounds over the sky

G-NILC can check if (# of foregrounds) $<$ (# of frequency channels)
→ diagnosis on the quality of the separation

Maps of the number of polarized foregrounds

B mode polarization

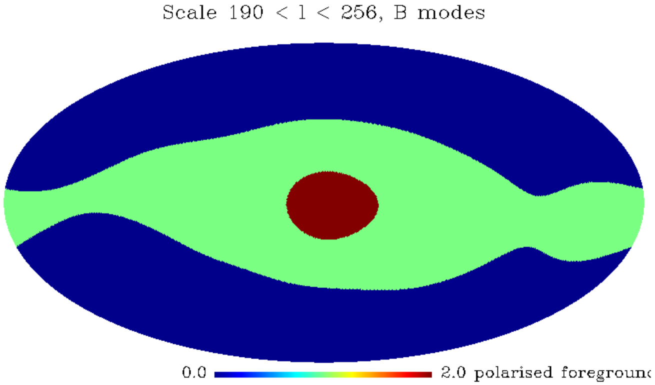

G-NILC able to provide maps of the number of polarized d.o.f over the sky

Maps of the number of polarized foregrounds

B mode polarization

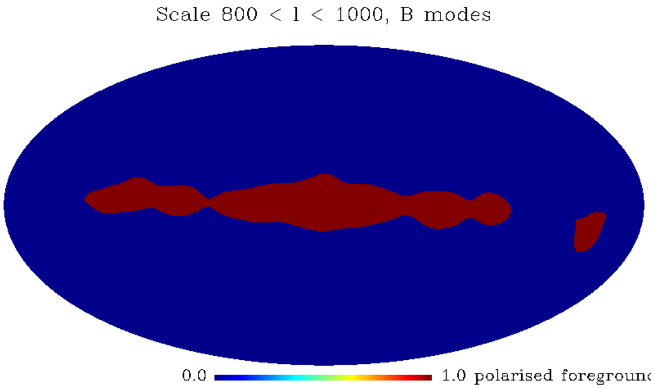

G-NILC able to provide maps of the number of polarized d.o.f over the sky

G-NILC can check if (# of foregrounds) < (# of frequency channels)
→ diagnosis on the quality of the separation

Impact on tensor-to-scalar ratio of incorrect foreground modelling with COrE/PRISM

with C. Dickinson, H.K Eriksen, I. Wehus *component separation, power spectrum estimation, parameter estimation*

- Parametric model Q/U: $\boldsymbol{s} = \left(\boldsymbol{s}^{cmb}, \boldsymbol{s}^{dust}, \boldsymbol{s}^{sync}\right), \boldsymbol{\beta} = (\beta_d, \beta_s, T_d), C_\ell = \langle |\boldsymbol{s}^{cmb}_{\ell m}|^2 \rangle$

$$\boldsymbol{d}(p) = a(\nu)\boldsymbol{s}^{cmb}(p) + \left(\nu/\nu_0^d\right)^{\beta_d(p)} B_\nu(T_d)\boldsymbol{s}^{dust}(p) + \left(\nu/\nu_0^s\right)^{\beta_s(p)} \boldsymbol{s}^{sync}(p) + \boldsymbol{n}(p)$$

- Joint CMB-foreground posterior distribution

$$P\left(\boldsymbol{s}, \boldsymbol{\beta}, C_\ell \middle| \boldsymbol{d}\right) \propto P\left(\boldsymbol{d} \middle| \boldsymbol{s}, \boldsymbol{\beta}, C_\ell\right) \underbrace{P\left(\boldsymbol{s}, \boldsymbol{\beta}, C_\ell\right)}_{\text{priors}}$$

- Gibbs sampling converges to sampling from the joint posterior $P\left(\boldsymbol{s}, \boldsymbol{\beta}, C_\ell \middle| \boldsymbol{d}\right)$

$$\boldsymbol{s}^{(i+1)} \leftarrow P\left(\boldsymbol{s} \middle| C_\ell^{(i)}, \boldsymbol{\beta}^{(i)}, \boldsymbol{d}\right)$$
$$C_\ell^{(i+1)} \leftarrow P\left(C_\ell \middle| \boldsymbol{s}^{(i+1)}\right)$$
$$\boldsymbol{\beta}^{(i+1)} \leftarrow P\left(\boldsymbol{\beta} \middle| \boldsymbol{s}^{(i+1)}, \boldsymbol{d}\right)$$

- Marginalized distribution of the CMB power spectrum

$$P\left(C_\ell \middle| \boldsymbol{d}\right) = \int P\left(\boldsymbol{s}, \boldsymbol{\beta}, C_\ell \middle| \boldsymbol{d}\right) d\boldsymbol{s}^{cmb} d\boldsymbol{s}^{dust} d\boldsymbol{s}^{sync} d\beta_d d\beta_s$$

$$\langle C_\ell \rangle = \int P\left(C_\ell \middle| \boldsymbol{d}\right) C_\ell dC_\ell = \frac{1}{N}\sum_{i=1}^{N} C_\ell^{(i)} \quad \Sigma = \frac{1}{N}\sum_{i=1}^{N}\left(C_\ell^i - \langle C_\ell \rangle\right)^2$$

Mismatch on the thermal dust emission law

Parametric model fitted

One modified blackbody ("one-component" dust)

Real sky

Two modified blackbodies ("two-component" dust) –Finkbeiner et al. (1999)

Because of the high-sensitivity of COrE-PRISM,
incorrect foreground modelling would likely be of major impact on (τ, r)

Impact on (τ, r) with PRISM and COrE channels

PRISM: 30, 36, 43, 51, 62, 75, 90, 105, 135, 160, 185, 200, 220, 265, 300, 320 GHz

COrE: 45, 75, 105, 135, 165, 195, 225, 255, 285, 315, 375 GHz

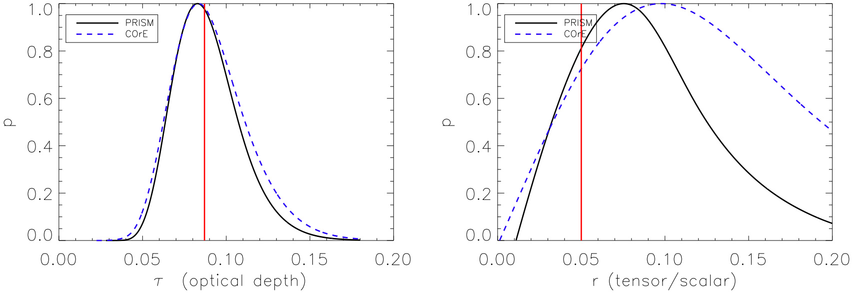

High-frequency channels of COrE/PRISM will be very helpful to highlight any failure in the model of thermal dust

Work plan with C. Dickinson, H.K Eriksen, I. Wehus

Mismatch tests between the simulated sky and the parametric model

- Incorrect number foreground degrees of freedom
  ex: omitted synchrotron curvature, two-component dust
  over-simplified / over-complicated model
- Additional polarized foregrounds
  (ex: spinning dust)
- Incorrect priors on foreground spectral indices

Impact on (τ,r) using Commander parametric fitting
on COrE, PRISM, EPIC, PIXIE, LiteBIRD simulations

In progress

Kinetic SZ & Relativistic thermal SZ

with J. Delabrouille, J.-B. Melin

CMB+KSZ extraction: standard ILC

TSZ input

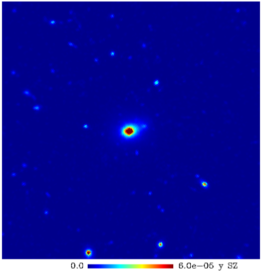

KSZ input

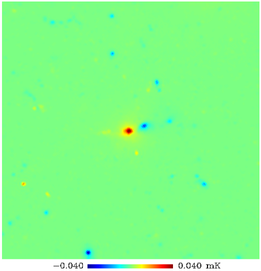

CMB input

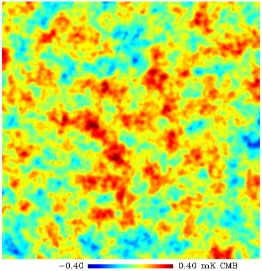

ILC (CMB+KSZ)

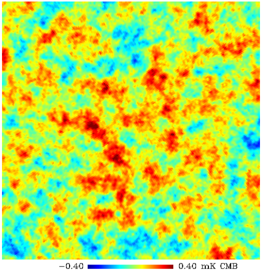

$$\boldsymbol{D}(\nu, p) = \boldsymbol{a}(\nu)\ S_{\mathrm{CMB}}(p) + \boldsymbol{b}(\nu)\ S_{\mathrm{tSZ}}(p) + \boldsymbol{n}(\nu, p)$$

Standard ILC $\quad \dfrac{a^T \mathrm{R}^{-1}}{a^T\ \mathrm{R}^{-1}\ a}$

Bennett et al., 2003, *Tegmark et al., 2003*,
Eriksen et al., 2004, *Delabrouille et al., 2009*

CMB+KSZ extraction: standard ILC

TSZ input

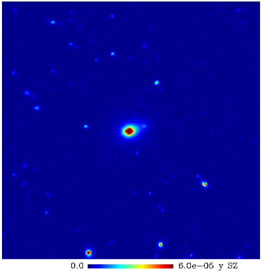

KSZ input

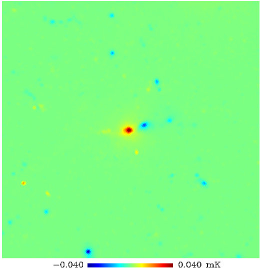

CMB input

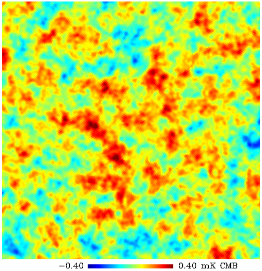

ILC - CMB

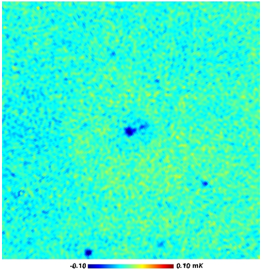

$$\boldsymbol{D}(\nu, p) = \boldsymbol{a}(\nu)\ S_{\rm CMB}(p) + \boldsymbol{b}(\nu)\ S_{\rm tSZ}(p) + \boldsymbol{n}(\nu, p)$$

Standard ILC $\quad \dfrac{\boldsymbol{a}^T \mathrm{R}^{-1}}{\boldsymbol{a}^T\ \mathrm{R}^{-1}\ \boldsymbol{a}}$

Bennett et al., 2003, *Tegmark et al., 2003*,
Eriksen et al., 2004, *Delabrouille et al., 2009*

CMB+KSZ extraction: 2D ILC

TSZ input

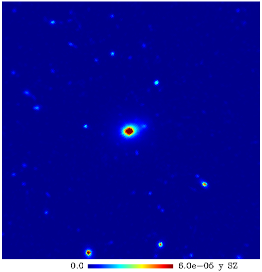

KSZ input

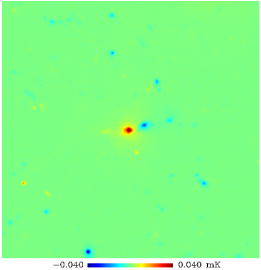

CMB input

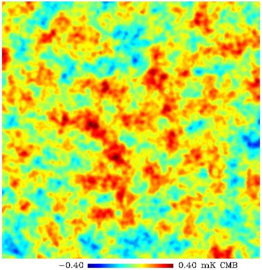

2D ILC - CMB

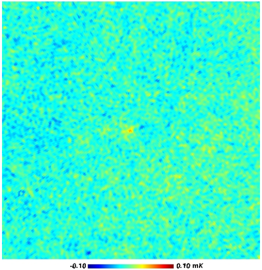

$$\boldsymbol{D}(\nu, p) = \boldsymbol{a}(\nu)\, S_{\mathrm{CMB}}(p) + \boldsymbol{b}(\nu)\, S_{\mathrm{tSZ}}(p) + \boldsymbol{n}(\nu, p)$$

2D ILC

$$\frac{\left(\boldsymbol{b}^T \mathrm{R}^{-1} \boldsymbol{b}\right) \boldsymbol{a}^T \mathrm{R}^{-1} - \left(\boldsymbol{a}^T \mathrm{R}^{-1} \boldsymbol{b}\right) \boldsymbol{b}^T \mathrm{R}^{-1}}{\left(\boldsymbol{a}^T \mathrm{R}^{-1} \boldsymbol{a}\right)\left(\boldsymbol{b}^T \mathrm{R}^{-1} \boldsymbol{b}\right) - \left(\boldsymbol{a}^T \mathrm{R}^{-1} \boldsymbol{b}\right)^2}$$

M. Remazeilles et al., “CMB and SZ Effect Separation with Constrained ILC”, MNRAS 410, 2481 (2011)

Relativistic corrections to the thermal SZ

Non-relativistic SED $\longrightarrow$ Relativistic SED

$$a_0(\nu) \longrightarrow a(\nu, T_e)$$

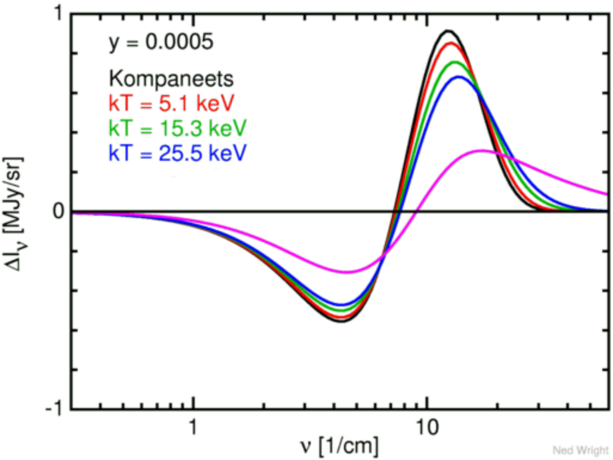

Relativistic SZ with 2D ILC

- Non-relativistic limit of thermal SZ SED

$$a_0(\nu) = \left(\frac{h\nu}{kT}\right)\coth\left(\frac{h\nu}{2kT}\right) - 4$$

- Relativistic thermal SZ

  Nozawa et al., ApJ 508 (1998): Taylor expansion in $\frac{K_B T_e}{mc^2}$ of the SED

$$\left(\frac{\Delta T}{T}\right)^{rel}_{SZ} \propto a(\nu, T_e) n_e T_e = a_0(\nu) n_e T_e + b(\nu) n_e T_e^2 + \ldots$$

Two components with two different SED!

→ The 2D ILC filter can separate the relativistic SZ

→ The relativistic SZ directly provides the temperature T_e of the clusters

In progress